5 Testing lepton universality, the $\pi \to e\overline{\nu}/\pi \to \mu\overline{\nu}$ branching ratio

P. Robmann, A. van der Schaaf, U. Straumann, P. Truöl and A. Palladino (guest from PSI/Virginia)

in collaboration with: University of Virginia, Charlottesville, USA; Institute for Nuclear Studies, Swierk, Poland; JINR, Dubna, Russia; Paul Scherrer Institut, Villigen, Switzerland and Rudjer Bošković Intitute, Zagreb, Croatia

(PEN Collaboration)

The measured value of the branching ratio

$$R_{e/\mu}^{\exp} \equiv \Gamma_{\pi\to e\overline{\nu}(\gamma)}/\Gamma_{\pi\to\mu\overline{\nu}(\gamma)} = 1.230(4)\times 10^{-4} \quad (1)$$

exhibits the best test of the universality of the coupling $Wl_i\nu_{l_i}$ (i=1,2,3 generation number) of the W boson to the leptons.

Within the Standard Model the decay $\pi \to e\overline{\nu}$ is helicity suppressed ($R_{e/\mu} \approx m_e^2/m_\mu^2/(1 - m_\mu^2/m_\pi^2)^2 \approx 1.3\times 10^{-4}$) which makes it sensitive to a number of hypothetical exotic contributions (2).

The PEN experiment aims at reducing the uncertainty for $R_{e/\mu}^{\exp}$ by an order of magnitude (3) which would bring it in the region of the present theoretical accuracy. See the Annual Report 2006/07 for further details on the theoretical motivation and a description of the PEN detection system.

5.1 Measurement principle

Determinations of $R_{e/\mu}$ are based on observing final states with positrons emerging from a stopped π^+ beam. Decays $\pi \to e\overline{\nu}(\gamma)$ result in positrons appearing with the pion lifetime (26 ns) and with an energy distribution peaking at $E_{e^+} = m_\pi c^2/2$. Decays $\pi \to \mu\overline{\nu}(\gamma)$ result in positrons too, through the subsequent decay $\mu \to e\nu\overline{\nu}$. The latter process leads to a time distribution first rising with the pion lifetime and then falling with the muon lifetime of 2.2 μs, and to a continuous energy distribution with $E_{e^+} \leq m_\mu c^2/2$. Whereas $\approx$ 98% of the $\pi \to e\overline{\nu}(\gamma)$ decays are unambiguously identified by their energy, in the remaining $\approx$ 2% the observed energy leaks into the region below $m_\mu c^2/2$ dominated by $\pi \to \mu\overline{\nu}(\gamma)$. For this reason it is crucial to know (measure and/or simulate) the full $\pi \to e\overline{\nu}(\gamma)$ energy distribution.

Random background from accidental pion-positron coincidences is suppressed by rejecting event topologies with nearby additional pion signals and the remaining background is extrapolated from events in which positrons are observed before a pion stop.

All measurements so far removed events in which the positrons appeared within a few ns after the pion stop time to suppress background processes originating in the abundant pion reactions with target nuclei. For our experiment such approach would require the knowledge of the time offset with a precision of $\approx$ 20 ps which would introduce a major source of systematic error. For this reason we decided to include the prompt region and control the prompt background by reducing the beam momentum and improving the event signature by a careful measurement of the pion energy deposition and range. For this purpose the pion energy loss is measured all along the trajectory with the help of active beam elements (plastic scintillator) read out with 2 GHz digitizers. The scheme not only helps to account for pion reactions but also for decays during the moderation process.

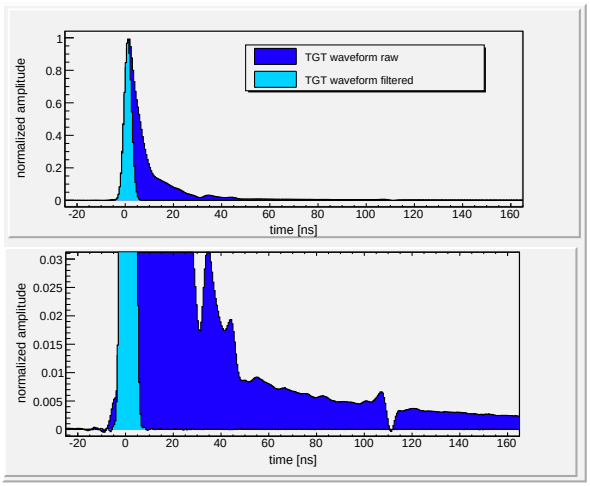

Figure 5.1: Raw and shaped target signals averaged over a very large number of pion interactions in the active target. The upper panel shows the full signal. In the lower panel the scale is reduced to show the structure in the signal tail. The shaping algorithm is explained in the text.

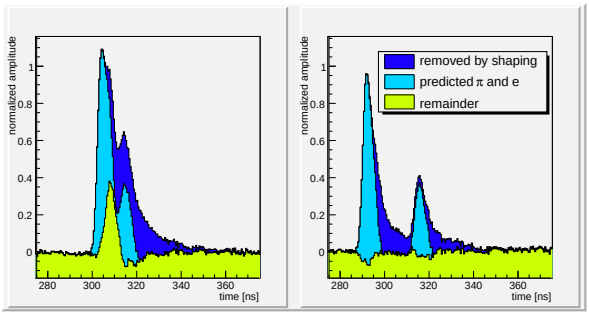

Figure 5.2:
Typical target waveforms for $\pi \to \mu \to e$ (left) and $\pi \to e\nu$ (right). Signals predicted for pion and positron are subtracted, as discussed in the text. For the $\pi \to e\nu$ event, the remaining signal is nil, while for the $\pi \to \mu \to e$ event, a 4 MeV muon is observed.

5.2 Target waveform analysis

Figure 5.1 shows the mean target waveform for pion reactions from a large sample of events before and after numerical shaping. The latter primarily removes distortions introduced by imperfect signal propagation (attenuation, dispersion, reflections) through the photomultiplier, cabling, splitters and mismatched terminators. The ≈ 0.5% structure after 110 ns, for example, is caused by an AC-coupled timing discriminator. One also notices a ≈ 0.5% shoulder in the leading edge which may result from crosstalk between the final dynodes of the photomultiplier.

The shaping is done in a single pass:

$$\tilde{w}_i = \sum_{k=k_{\min}}^{k_{\max}} s_k w_j,\ k \equiv i - j\ , \qquad (5.1)$$

where w and $\tilde{w}$ are the raw and shaped waveforms, respectively, and s_k is an array of coefficients trained to make $\tilde{w}$ approach a Gaussian distribution with $\sigma = 1.5$ ns as closely as possible (4). The shaping interval $(k_{\min}, k_{\max})$ roughly coincides with the region shown in Fig. 5.1. One should keep in mind that the scintillation signal has an intrinsic fall time of ≈ 2 ns only so there is no significant loss in statistical accuracy of the associated energy signal. We believe the method described is novel [4] certainly in the fields of particle and nuclear physics.

Figure 5.2 shows examples of target waveforms for the two decay modes. The waveform discrimination is done by comparing χ^2 values of waveform fits with and without an intermediate muon. Since pulses may appear almost simultaneously additional constraints on the amplitudes of the particles involved are included in the χ^2 expressions for the two hypotheses:

- **E_μ**
  The energy of the mono-energetic muon is fixed to 4.1 MeV from 2-body kinematics.

- **t_π and t_e**
  Pion and positron times are fixed to the values deduced from the degrader and the

[4] Similar problems occur in totally different areas such as acoustics and seismology but so far we didn't find treatments as rigorous as ours

plastic hodoscope, respectively.

- E_π
  Pion energy in the target can be predicted from the kinetic energy deduced event-by-event from the pion time of flight over the final 3.5 m of the beamline after correction for the observed energy loss in the degrader. Figure 5.3 shows the correlation between predicted and observed pion energies in the target, which is small on the scale of the 4.1 MeV muon.

- E_e
  The positron energy scales with the positron path length in the target, which can be deduced from the observed positron and pion trajectories (see below). As in the case of the pion the deviation from the predicted value, normalized to the uncertainty, is included. In the $\pi \to \mu \to e$ fit the uncertainty is affected by the 1.5 mm distance traveled by the muon.

The above considerations lead to the following extended χ^2 expression:

$$\chi^2 = \frac{1}{n_{\mathrm{d.o.f.}}} \sum_{i=1}^{n} \left(\frac{\tilde{w}_i^{\mathrm{fit}} - \tilde{w}_i}{\sigma_{\tilde{w}}} \right)^2 + \left(\frac{E_\pi^{\mathrm{fit}} - E_\pi^{\mathrm{pred}}}{\sigma_{E_\pi}} \right)^2 + \left(\frac{E_e^{\mathrm{fit}} - E_e^{\mathrm{pred}}}{\sigma_{E_e}} \right)^2 ,$$

where $\tilde{w}$ was introduced in Eq. 5.1. The summation is limited to the n bins of $\tilde{w}_i$ which receive contributions from the $\pi \to \mu \to e$ fit so n varies depending on the amount of overlap between the three peaks. The number of degrees of freedom $n_{\mathrm{d.o.f.}}$ equals n-2 and n-3 for the fits to $\pi \to e\nu$ and $\pi \to \mu \to e$, respectively. σ_{E_π}=0.6 MeV and σ_{E_e} is distributed according to the asymmetric energy-loss distribution.

Figure 5.4 shows preliminary results for the χ^2 difference between the two decay hypotheses indicating a separation of better than 1:100 based on waveform analysis alone.

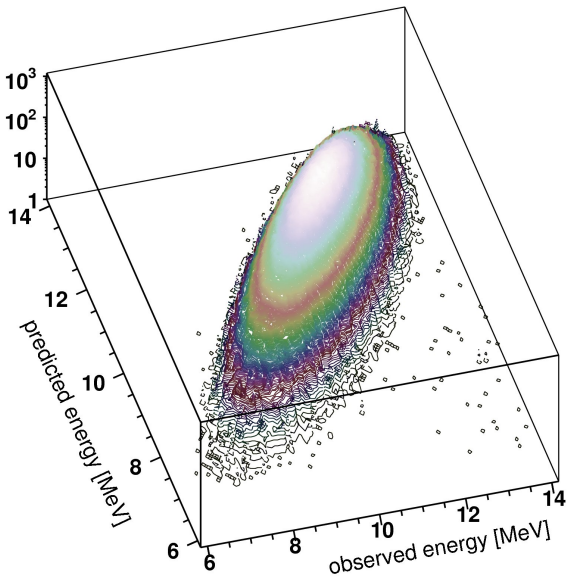

Figure 5.3:
Distribution of observed versus predicted pion energy in the target. The predicted energy is the kinetic energy deduced from the measured pion velocity corrected for the observed energy loss in the degrader.

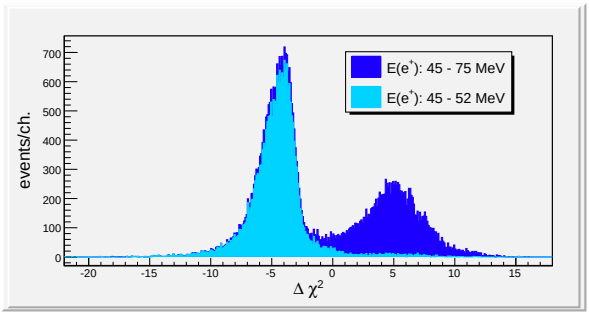

Figure 5.4:
Distributions of the difference in χ^2 with/without intermediate muon. Events were selected in which the positron appeared within 75 ns after the pion stop. Note the contribution in the lower-energy interval with $\Delta\chi^2 \approx 5$ which is expected from the low-energy tail of the $\pi \to e\nu$ response.

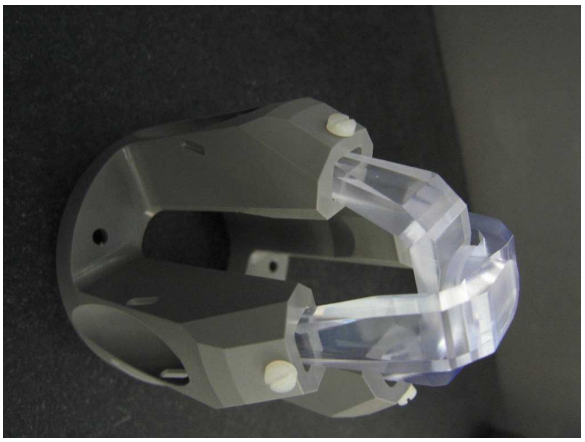

Figure 5.5: The four-plane wedged degrader used in 2008 to measure the pion trajectory before wrapping. The beam enters from the left.

5.3 A poor man's beam tracker

The determination of the decay vertex requires the tracking of both the positron and the pion. In future running, the pion tracking will be done with a mini-TPC which is presently being tested. Halfway during the 2008 data-taking we installed as an intermediate solution a fourfold segmented degrader (see Fig. 5.5) which was produced in our mechanical workshop.

Depending on the pion position in the transverse plane, the energy loss in the four detector elements varies which allows position determination. Unfortunately, the 12 mm thick detector significantly affects the pion trajectories by multiple scattering resulting in a relatively poor ($\sigma \approx 2$ mm) vertex resolution. It also appears that the light collection shows significant position dependence which had to be taken into account numerically.

5.4 Outlook

A second four-month period of data-taking has been scheduled for the end of 2009. As mentioned above, we will use a new mini-TPC for pion tracking. This detector will be situated between the degrader and the target. This modification in the setup will not only lead to a dramatic improvement in vertex resolution, but also allow for a 10% reduction in beam momentum which will result in improved time-of-flight resolution and thus a lower σ_{E_π}.

Meanwhile we will proceed with the analysis of the 2008 data. Presently we are developing the framework of a sophisticated likelihood analysis of all observables discussed above. In addition to the two main signal processes, a series of other event types have to be included to push the systematic error in the branching ratio well below 10^{-3}. Radiative decays, in-flight decays, various types of accidental coincidences and pion reactions have been identified so far. It is our aim to determine all probability density functions directly from the measurement. To help access systematic uncertainties, detailed Monte Carlo studies have recently been initiated.

[1] G. Czapek $\mathrm{et\ al.}$, Phys. Rev. Lett. **70** (1993) 17; D. I. Britton $\mathrm{et\ al.}$, Phys. Rev. Lett. **68** (1992) 3000.

[2] M. Raidal and A. van der Schaaf $\mathrm{et\ al.}$, Eur. Phys. J. C **57** (2008) 13 [arXiv:0801.1826 [hep-ph]].

[3] PEN Collaboration, PSI experiment R-05-01, D. Pocanic and A. van der Schaaf, spokespersons.

[4] A. Palladino, D. Pocanic and A. van der Schaaf, in preparation.